Robustness to Mutations Depends on whether RNA Virus Replication Occurs Geometrically or Via a Stamping Machine

Josep Sardanyés
Ricard V. Solé
Santiago F. Elena

SFI WORKING PAPER: 2008-12-050

SFI Working Papers contain accounts of scientific work of the author(s) and do not necessarily represent the views of the Santa Fe Institute. We accept papers intended for publication in peer-reviewed journals or proceedings volumes, but not papers that have already appeared in print. Except for papers by our external faculty, papers must be based on work done at SFI, inspired by an invited visit to or collaboration at SFI, or funded by an SFI grant.

©NOTICE: This working paper is included by permission of the contributing author(s) as a means to ensure timely distribution of the scholarly and technical work on a non-commercial basis. Copyright and all rights therein are maintained by the author(s). It is understood that all persons copying this information will adhere to the terms and constraints invoked by each author's copyright. These works may be reposted only with the explicit permission of the copyright holder.

www.santafe.edu

SANTA FE INSTITUTE

Robustness to Mutations Depends on whether RNA Virus Replication Occurs Geometrically or Via a Stamping Machine

Josep Sardanyés,[1,*] Ricard V. Solé,[1,2] and Santiago F. Elena[3,2]

[1]*Complex Systems Lab (ICREA-UPF), Barcelona Biomedical Research Park (PRBB-GRIB) Dr. Aiguader 88, 08003 Barcelona, Spain*

[2]*Santa Fe Institute, 1399 Hyde Park Road, Santa Fe NM 87501, USA*

[3]*Instituto de Biología Molecular y Celular de Plantas, CSIC-UPV, Ingeniero Fausto Elio s/n, 46022 València, Spain*

Regardless genome polarity, during viral replication intermediaries of complementary sense must be synthesized and used as templates for the synthesis of new genomic strands. Depending on whether the newly synthesized genomic molecules become themselves templates for producing extra antigenomic strands, thus giving rise to a geometric growth, or only the firstly synthetized antigenomic strands can be used to this end, thus following Luria's stamping machine model, the abundance and distribution of mutant genomes will be different. Mathematical models of virus replication have largely ignored this fact and generally assumed a pure geometric growth. Here we propose mathematical and bit string quasispecies models that allow to distinguish between linear and geometric replication and also incorporating the existence of antigenomic intermediates of replication. We have observed that the error threshold increases as the mechanism of replication switches from purely geometric to stamping machine. We also found that for a wide range of mutation rates, large effect mutations do not accumulate regardless the scheme of replication. However, mild mutational effects accumulate more in the geometrical mode. Furthermore, at high mutation rates, geometric growth leads to a sooner population collapse for intermediate values of mutational effects at which the stamping machine still produces non mutated genomes. Finally, at increasing mutation rates, the highest production of virions is found for close-to-linear replication and high replicase production. In conclusion, we have shown that by selecting a stamping machine replication strategy, RNA viruses may increase their robustness against the accumulation of deleterious mutations.

The mode of RNA virus replication has important consequences for understanding the rates at which deleterious mutations accumulate and the statistical properties of the cloud of mutants around the master sequence (1, 2). For the sake of illustration, let's assume that the infecting virus has a mRNA sense (positive strand) genome, such as for example the picorna-like viruses. The different steps of the infectious cycle are illustrated in Figure 1. The first step of infection would be the uncoating of the RNA molecule, followed by its translation to produce viral proteins, including one or more required to generate the RNA-dependent RNA polymerase (RdRp) that serves as replicase. The replicase then copies the genomic strand to make antigenomic (negative polarity) strands. These are used as templates to produce the positive strand progeny that will accumulate in the cell, serve as templates for translation and, following encapsidation by coat proteins, form new virions. If the antigenomic strands produced during the first round of synthesis are the only templates for producing the entire progeny of genomic positive strands, the distribution of mutations per genome within an infected cell is expected to be Poisson because mutants do not replicate. Consequently, the fraction of mutation-free genomes produced is given by the Poisson null class $e^{-\mu L}$, where μ is the per site mutation rate and L the genome length. This scheme of replication corresponds to the linear stamping machine model first proposed by Luria (3).

*Corresponding author. Mailing address. Complex Systems Lab (Universitat Pompeu Fabra), PRBB, Barcelona, 08003. E-mail: josep.sardanes@upf.edu; Phone:+34 933160532; Fax: +34 933160550

However, if all positive strand progeny can also immediately serve as templates for additional rounds of antigenomic strands synthesis, the replication model is effectively geometric and the distribution of mutant genomes per cell increases in variance because mutant progeny is producing itself more mutant viruses. In this case, the distribution of mutant genomes conforms to the Luria-Delbrück distribution (4). The fraction of mutation-free genomes produced would depend on the number of replication rounds experienced, k, according to $e^{-k\mu L}$. If only a fraction of the positive strand progeny replicates, then the replication model will be a mixture of geometric growth and stamping machine that deviates from the Poisson expectation as much as the geometric growth contribution. The effect of replication mode in virus mutational load can be better understood with the following example. The genomic mutation rate of the positive strand *Tobacco mosaic virus* (TMV) was estimated in the range $0.043 \leq \mu L \leq 0.063$ per replication round and about 40 viral particles produced per infected tobacco cell (5). For a pure stamping machine model, the fraction of mutation-free genomes would be in the range $0.939 - 0.958$, whereas for a pure geometrical growth ($k = 5.322$) this fraction would lie between 0.795 and 0.715. Therefore, geometric replication produces $4.666-4.860$ times more mutants than a stamping machine model.

Experimental data suggest different models of replication for different viruses. For example, bacteriophage $T2$ is thought to replicate mostly following a geometric model because the number of mutants per infected cell fails to fit a Poisson distribution (3). However, phage $\phi X174$ data fit well the Poisson distribution and, hence, is thought to replicate according to a stamping machine model (6). Lying within these

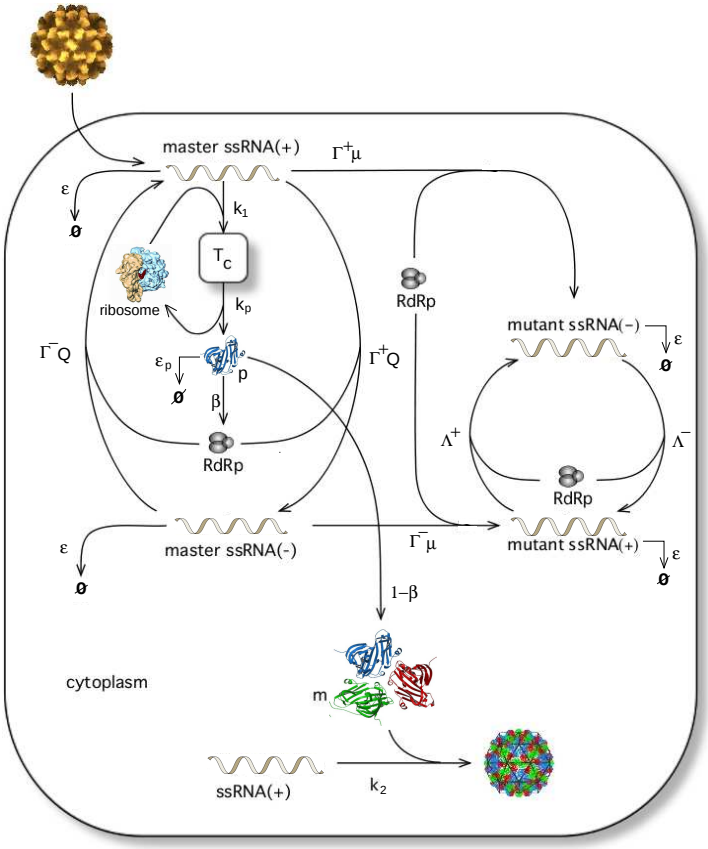

FIG. 1: Schematic representation of the virus infectious cycle. During infection, the viral particle enters into the host cell and after uncoating, the positive-sense RNA (acting as mRNA) forms the translational complex, T_c, by binding with ribosomes, that directs the synthesis of the viral polyprotein precursor, p, which is converted to both structural and RdRp proteins, at rates $1-\beta$ and β, respectively. The RdRp is used to synthesize more copies from the viral RNA templates. We distinguish between master and mutant genomic $(+)$ and antigenomic $(-)$ strands. We simulate linear replication with $\Gamma^+ \ll \Gamma^-$ (where the initial genomic RNA directs the synthesis of one or very few negative copies which are used as templates for the synthesis of new genomic strands). To model geometric replication we use $\Gamma^+ = \Gamma^-$, where all the synthesized strands replicate at the same rate. We also model the formation of mature viral particles from genomic strands and the structural proteins (see Table I for a description of the variables and the parameters used in the model).

two extremes, phage $\phi 6$ slightly deviated from the Poisson expectation, an observation interpreted as result of a mixed model in which some progeny was also able of replicating (1). Plant positive strand RNA viruses are also thought to replicate mostly according to a stamping machine model (2, 7). Despite the apparent importance of the model of RNA virus replication on the accumulation of mutant genomes, most of the mathematical models proposed to study the dynamics of RNA virus populations rely on the assumption of geometric growth. For example, the most commonly used theoretical paradigm for the study of virus evolution, Eigen's quasispecies model (8, 9), assumes geometric growth without making specific mention to the genomic-antigenomic duality.

How to model viral replication is a current subject of research in virology. The growth of a virus in its host cell is a complex process. In seeking to understand this process and the effect of the interactions between the macromolecules involved in viral growth, the crossing of disciplines as biochemistry, molecular biology, population genetics and nonlinear dynamical systems might provide a powerful way to study the overall behavior of virus dynamics. In this sense, models play a crucial role for a qualitative and a quantitative study of virus replication, being also useful to predict the system's behavior time evolution as well as to analyze its sensitivity with respect to parameter changes. Furthermore, insights into interactions of viruses with host cells might help us to improve our understanding of virus-mediated diseases and to develop antiviral strategies (10). Several models of intracellular viral growth kinetics can be found in the literature, ranging from simple (unstructured) models capturing the basic replication processes (11–14) to the so-called structured models that consider replication in different cellular compartments such as membranes, endosomes, cytoplasm or nucleus. Some examples of structured models have been developed for bacteriophage $T7$ (15, 16), *Human immunodeficiency virus* type 1 (17), subgenomic *Hepatitis C virus* (18), *Influenza A virus* (10) or *Vesicular stomatitis virus* (19). However, to the extent of our knowledge and despite its relevance, none of the above theoretical models incorporate antigenomic strands synthesis as intermediates of replication considering the effect of non-

Category	Notation	Description
Parameters	β	Fraction of the viral polyprotein used as replicase, being $1-\beta$, the fraction used as structural proteins
	ε	Strand's degradation rate
	ε_T	Degradation rate of the translational complex*
	ε_p	Degradation rate of the viral polyprotein*
	$\Gamma^{\pm}$	Replication rate for the positive $(+)$ (genomic) and negative $(-)$ (antigenomic) master strands
	$\Lambda^{\pm}$	Replication rate for the positive and negative mutant strands
	$\mathcal{K}$	Cellular carrying capacity or maximum populations size of strands per cell*
	k_p	Effective interaction rate between the master genomic strands and the available ribosomes*
	k_1	Dissociation rate of the genomic master strand from the translational complex*
	k_2	Encapsidation rate of positive-sense strands
	m	Number of monomers of structural protein used for building up a virion*
	Q	Average copying fidelity, being $\mu = 1 - Q$ the mutation rate
	R^{tot}	Constant number of cellular ribosomes inside the cell*
	σ	Rate of elimination of mature virions (either by degradation or by licking out of the cell)
State variables	$x_0^{\pm}$	Relative concentration of genomic and antigenomic master strands
	$x_1^{\pm}$	Relative concentration of genomic and antigenomic mutant strands
	T_c	Relative concentration of translational complexes composed of master genomic strands and ribosomes
	p	Relative concentration of the non-processed polyprotein
	V	Relative concentration of mature virions

TABLE I: Notations used in the ODEs model. Asterisks indicate the fixed parameters (see the end of the mathematical model description for exact values).

geometric modes of replication on viral mutational load.

In this work we first analyze a quasispecies structured model describing the single-cell reproductive cycle of positive-sense RNA viruses that make no subgenomic mRNAs and encodes a single polyprotein that is self-processed into structural and non-structural proteins, sensu picorna-like viruses (see Figure 1). Our model describes the dynamics of cytoplasmatic intracellular amplification of the viral strands considering the main mechanisms involved in the infection cycle inside the host cell (see (20) and references therein). Our main goal is to analyze the effect of linear and geometric replications under a single-peak fitness landscape (21). We are especially interested in the error threshold and the sensitivity to mutations for each replication mode. The model considers explicitly both genomic and antigenomic master and mutant strands, the viral polyprotein precursor, the translational complexes and the mature virions.

Our results show that geometric replication is more sensitive to the error catastrophe, as opposed to the Luria's stamping machine strategy, which is shown to occur at higher mutation rates. We confirmed the validity of the results obtained with the mathematical deterministic model by using a stochastic model involving digital genomes.

MATERIALS AND METHODS

Mathematical model. Our quasispecies mathematical model of intracellular viral replication is based on the replication scheme shown in Figure 1 (see Table 1 for details on notation used hereafter). The model is used to analyze the dynamics of replication of positive-sense RNA viruses that make no subgenomic mRNAs. We explicitly define the polarity of the strands constituting the quasispecies, studying its dynamics using the so-called Swetina-Schuster landscape (21), which assumes that all mutations have the same deleterious effect on virus fitness. In such scenario we may divide the population in either master or mutant positive and negative viral strands. The pool of mutant strands of each polarity is thus grouped in an average sequence different from the master one. Therefore, the state variables (which have real positive values) of this dynamical system are given by the genomic $(+)$ and antigenomic $(-)$ viral strands, $x_{0,1}^{\pm}$, being the master ones indicated with subindex 0 and the mutants with subindex 1. Moreover we also consider as state variables the viral polyprotein precursor, p, the translation complex, T_c, and the virions, V.

Our model assumes that all the interacting macromolecules are homogeneously mixed, also assuming that mutant genomic RNAs (x_1^+) are not translated to produce the polyprotein precursor and thus they do not compete for the available ribosomes. This may happen because mutations could produce a stop codon or a sort of conformational change in the secondary structure of the RNA hindering its binding with the ribosomes. Next we proceed to give a detailed explanation of the processes described by our model. We mainly differentiate four steps, (a) to (d) below, which correspond to the main phases of viral replication inside the host cell (Figure 1).

(a) *Translation complex kinetics*. Upon entry and uncoating of the viral genome, it binds with the cellular ribosomes forming the translational complexes. Following Dahari and co-workers (18), the amount of free available ribosomes, R^{av}, is used as an upper bound to the formation of the translation complexes, T_c, and is given by $R^{av} = R^{tot} - T_c$. Note that here we assume that the total number of ribosomes, R^{tot}, is constant, and the number of available ribosomes decreases due to the formation of the translational complexes. The dynamics of the translational complex is then defined by

$$\frac{dT_c}{dt} = k_p x_0^+ R^{av} - k_1 T_c - \varepsilon_T T_c. \tag{1}$$

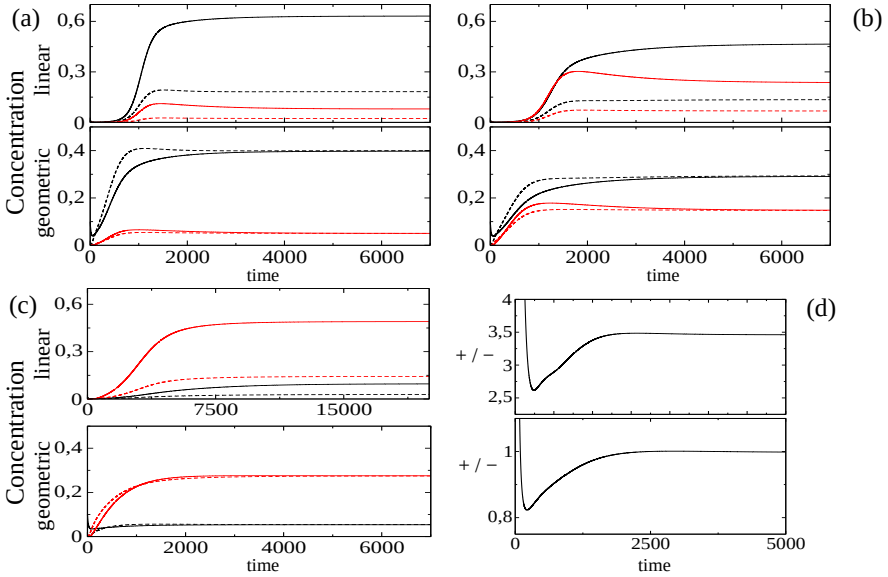

FIG. 2: Solutions of the ODEs model. Time series for master (black) and mutant (red) strands at different mutation rates and with $\varepsilon = 10^{-3}$. The mutation rates analyzed are: (a) $\mu = 0.1$; (b) $\mu = 0.3$; and (c) $\mu = 0.75$. Positive and negative-sense strands are indicated, respectively, with solid and dashed lines. We also show the ratio of positive to negative strands for the case $\mu = 0.3$. In all the plots we show the time evolution for linear (upper panel, with $\Gamma^+ = 0.1$) and geometric (lower panel, with $\Gamma^+ = 1$) replication modes.

Here the parameter k_p is the effective interaction rate between the RNA and the available ribosomes. The second term denotes the dissociation of the translation complex and the master genomic RNA strands ($k_1 T_c$), after which the ribosomes and the genomic RNA become again available for the replicative cycle. We consider that the translation complex is degraded at rate ε_T.

(b) *Viral polyprotein precursor dynamics*. The dynamics of the viral polyprotein precursor, p, is dependent on the presence of the complexes, T_c, the formation of mature virions and its intrinsic degradation. An appropiate description reads

$$\frac{dp}{dt} = k_1 T_c - \sum_{i=0,1} \varphi(x_i^+) - \varepsilon_p p. \tag{2}$$

The φ term, which corresponds to the formation of virions due to the encapsidation of the positive-sense strands, is chosen here as $\varphi(x_i^+) = k_2[(1-\beta)p]^m x_i^+$, with $i = 0, 1$. Here k_2 is the encapsidation rate, and m the number of monomers of structural protein used for the encapsidation of the genomic strands.

The viral polyprotein precursor is proteolitically self-processed giving place to the formation of both structural (capside proteins) and non-structural (replicase) proteins, which are synthesized, respectively, at rates $1-\beta$ and β (12). The last term indicates the degradation of the viral polyprotein proportionally to ε_p.

(c) *RNA synthesis and degradation*. Four different classes of RNA sequences defined as $x_j \in \{x_0^+, x_0^-, x_1^+, x_1^-\} = \mathbf{x}$, are considered and their growth is limited by a logistic-like term given by

$$\mathcal{L}(\mathbf{x}) = 1 - \frac{1}{\mathcal{K}} \sum_{i=0,1} (x_i^+ + x_i^-),$$

together with a linear degradation $-\varepsilon x_j$, describing the decay of viral strands due to the action of the cellular endonucleases, which is assumed to be the same for all strands. The constant $\mathcal{K}$ corresponds to the cellular carrying capacity or the maximum population of viral strands that can be produced inside the host cell. The RdRp uses a given strand as template to synthesize its perfectly complementary sequence at a rate $\Gamma^{\pm} Q$, being Q the average quality factor of replication and $\Gamma^{\pm}$ the replication rate of the master strands. Hence, master sequences will generate mutant complementary sequences at a rate $\Gamma^{\pm}\mu$, being $\mu = 1 - Q$, the average mutation rate. Mutant strands replicate at rates $\Lambda^{\pm} \ll \Gamma^{\pm}$ because we assume that mutants are deleterious. Note that backward mutations are not allowed to occur due to the enormous size of sequence space.

The concentration of free x_0^+ strands will grow following:

$$\frac{dx_0^+}{dt} = r_+ \mathcal{L}(\mathbf{x}) - \varepsilon x_0^+ + k_1 T_c - \varphi(x_0^+) - k_p R^{av} x_0^+, \tag{3}$$

where the three last terms in the right-hand side correspond to the dissociation from the translation machinery ($k_1 T_c$), the sequestration rate $\varphi(x_0^+)$ due to the formation of new viral particles, and the capture from free ribosomes to produce new translational complexes, respectively. The growth rate r_+ incorporates the presence of x_0^- templates, the fraction of the viral polyprotein, p, used as replicase (βp), and the quality factor of replication, Q, with $r_+ = \Gamma^- Q x_0^- \beta p$. For the strands x_0^-, the dynamics is now given by

$$\frac{dx_0^-}{dt} = r_- \mathcal{L}(\mathbf{x}) - \varepsilon x_0^-, \tag{4}$$

where now $r_- = \zeta(\mathbf{x}^-)\Gamma^+ Q x_0^+ \beta p$, (see below for the expression of $\zeta(\mathbf{x}^-)$). Similarly, we can build the equations for the mutant populations as follows

$$\frac{dx_1^+}{dt} = r'_+ \mathcal{L}(\mathbf{x}) - \varphi(x_1^+) - \varepsilon x_1^+, \tag{5}$$

and

$$\frac{dx_1^-}{dt} = r'_- \mathcal{L}(\mathbf{x}) - \varepsilon x_1^-, \tag{6}$$

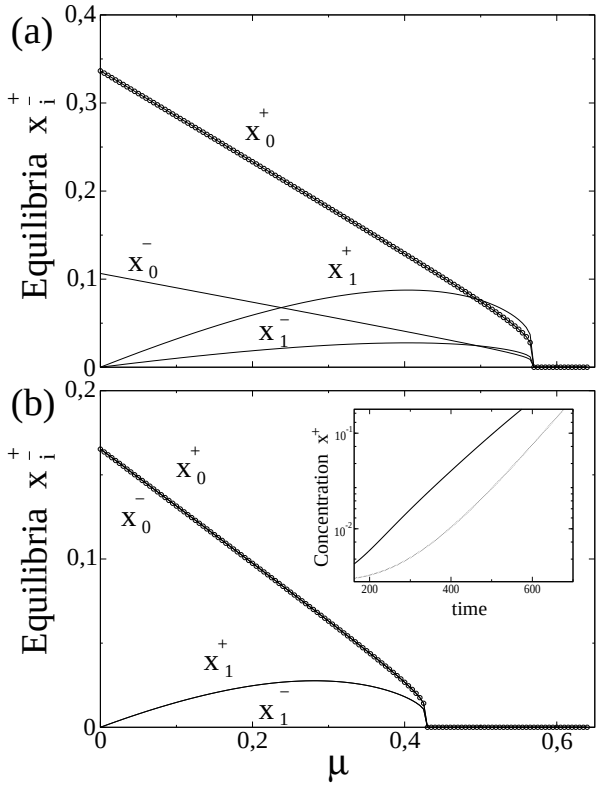

FIG. 3: Equilibrium concentrations for master ($x_0^{\pm}$) and mutant ($x_1^{\pm}$) strands against mutation rate, $\mu = 1 - Q$, for linear (a) and geometric (b) replication with $\varepsilon = 0.01$. The inset displays the initial amplification phase of the genomic RNA strands ($\mathbf{x}^+ = x_0^+ + x_1^+$, in linear-log scale) undergoing geometric (solid line) and linear (dotted line), using $Q = 0.9$ and $\varepsilon = 10^{-4}$. As initial conditions we used $x_0^+(0) = 0.01$ and $x_0^-(0) = x_1^{\pm}(0) = p(0) = T_c(0) = 0$. For linear replication we used, in all the plots, $\Gamma^+ = 0.1$, while for geometric replication we used $\Gamma^+ = 1$. In all these analyses we used $\beta = 1$ and $\sigma = 0$.

with their replication rates now given by $r'_+ = [\Gamma^-(1-Q)x_0^- + \Lambda^- x_1^-]\beta p$, and $r'_- = \zeta(\mathbf{x}^-)[\Gamma^+(1-Q)x_0^+ + \Lambda^+ x_1^+]\beta p$, consistently with the reactions outlined in Figure 1.

(d) *Formation of viral particles*. The new virions are produced from both master and mutant genomic strands combined with the structural proteins. From the previous steps, we can see that the formation of mature virions, V, will follow

$$\frac{dV}{dt} = \sum_{i=0,1} \varphi(x_i^+) - \sigma V. \tag{7}$$

Where the left-hand side term represents the encapsidation of positive strands and the last term (σV) is introduced to control the amount of virions (e.g., degradation of viral particles and elimination of mature particles that may lick out the cell).

Note that the differences in the replication rates of both genomic and antigenomic strands allow us to analyze linear (stamping machine) and geometric replication kinetics. To model geometric replication we set $\Gamma^+ = \Gamma^-$, i.e., all the synthesized strands are allowed to replicate. For linear kinetics, however, we use $\Gamma^+ \ll \Gamma^-$, that is, the infectious genomic RNA entering into the host cell synthesizes one or very few negative copies which are then used as the only templates for the synthesis of new ssRNA+ strands in a Luria's stamping machine strategy. Indeed, to further stress the assumption that at the beggining of the infectious cycle only the antigenomic strands need to be produced but as infectious progresses, this production has to be shut off to favor production of genomic strands, we assume a negative feedback of antigenomic strands concentration on its own rate of production. In mathematical terms, this contraint can be incorporated by setting $\zeta(\mathbf{x}^-) = 1/(1 + x_0^- + x_1^-)$ in the production of antigenomic strands from genomic ones. For geometric replication $\zeta(\mathbf{x}^-) = 1$.

For the sake of simplicity we hereafter will use (by default): $\Gamma^- = 1$, $\Lambda^{\pm} = \Gamma^{\pm}/10$ (i.e., assuming that mutants are largely deleterious and have reduced replication rate in a factor of $1/10$), $k_p = 0.04$, $k_1 = 0.02$, $\varepsilon_T = 10^{-5}$, $\varepsilon_p = 0.0015$, $m = 2$, $R^{tot} = 1$ and $\mathcal{K} = 1$. The other parameters will be explored in this work. Hereafter we will also assume that a strand extincts if $x_{0,1}^{\pm} < 10^{-18}$. The initial conditions for the seven state variables are set to $x_0^+(0) = 0.1$ and $x_0^-(0) = x_1^{\pm}(0) = p(0) = T_c(0) = V(0) = 0$ (if not otherwise specified).

Stochastic digital genomes. During the first stages of the infection and due to the stochastic nature of transmission events, cells are usually invaded by one or few viral particles. Therefore, a stochastic description of the replication process would better capture the fluctuations due to small population sizes (see (13) and references therein). We use an unstructured discrete model of *in silico* genome evolution considering a bit string description of the population structure (22, 23) which allows us to explicitly simulate the complex and heterogeneous structure of populations of replicators. Although a real RNA is composed by a four-letter alphabet, we use Leuthäusser approach by considering that each bit would represent purines or pyrimidines (24, 25). Our digital strands will thus be represented as chains of bits. Each chain will have $\nu = 32$ bits and a maximum population size of $N = 1000$ chains will be allowed.

We define a population of strings, Ω, representing digital genomes. We indicate as S_i^+ and S_i^- positive and negative strands, respectively. A given string will be defined as $S_i^{\pm} = (S_{i1}^{\pm}, S_{i2}^{\pm}, ..., S_{i\nu}^{\pm})$, with $S_{ik}^{\pm} \in \{0, 1\}$. The genomic and antigenomic master sequences in our model (indicated as S_m) are chosen to be $S_m^+ = (11...1)$ and $S_m^- = (00...0)$, respectively. We initially "inoculate" our system with $N(0)$ genomic replicating strings, S_m^+. These strings can now replicate (generating complementary strands) and mutate. For instance, each bit in S_i^+ can mutate, i.e., $S_{ik}^+ \xrightarrow{\mu_b} 1 - S_{ik}^+ = S_{ik}^-$, with a given mutation probability per bit μ_b and replication cycle. They also degrade with probability ε. The master sequences have the highest fitness: their replication probabilities are $\Gamma^{\pm}$ whereas all other strings replicate with a probability $\Lambda^{\pm} = 0.1$). This defines a sharp, single-peak fitness landscape (21), as used in the previous mathematical model. The simulation algorithm repeats, at every generation τ, $N = 10^3$ times the replication and degradation rules. This updating ensures that, on average, the rules are applied to all the population of strings.

To differentiate between both types of replication we follow the next strategy: when a positive strand replicates producing a negative one, the latter will always keep replicating (unless degraded). On the contrary, when a negative strand replicates, the synthesized positive strand will become a replicator with probability $\rho \in [0, 1]$. Note that with $\rho = 1$ all the progeny strands copied from the negative templates will replicate in the following generations and replication will be purely geometric. However, with $\rho \ll 1$, the negative strands

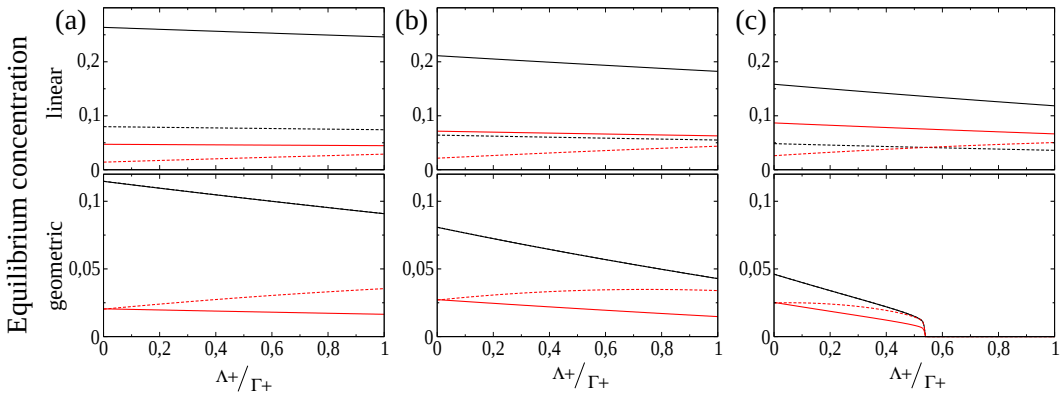

FIG. 4: Severity of mutations and accumulation of strands. Relative effect of mutations on the equilibrium concentration of the strands using the ratio Λ^+/Γ^+ (with $0 \leq \Lambda^+/\Gamma^+ \leq 1$) as control parameter, with $\varepsilon = 0.01$, $\beta = 1$, and: $\mu = 0.15$ (a); $\mu = 0.25$ (b); and $\mu = 0.35$ (c). In all the plots we represent (upper) linear replication using $\Gamma^+ = 0.1$ (with $0 \leq \Lambda^+ \leq 0.1$) and (lower) geometric replication with $\Gamma^+ = 1$ (with $0 \leq \Lambda^+ \leq 1$).

will be mainly used as templates while the positive ones will not replicate. With this second strategy the kinetics will be closer to the Luria's stamping machine. Indeed, to potentiate the effect of linear replication, the non-replicating positive strands are not degraded, and the degradation probability for the replicating sequences is kept very low. We also consider differential replication rates for each strategy of replication, by using $\delta\Gamma^+$ and $\delta\Lambda^+$. For linear replication we set $\delta = 0.1$, where the positive-sense strands will synthesize few negative ones. For geometric replication we use $\delta = 1$, and all the synthesized strands will be used as templates for further replication.

All numerical analysis of the ODEs model were done using a C program implemented to solve the differential equations with the standard fourth order Runge-Kutta method (26) using a constant time step size of $\Delta t = 0.1$. The stochastic bit string model was also implemented in a C program whose code is available upon request.

RESULTS

Mathematical model

Quantitative differences in the accumulation of master and mutant genomes of both polarities The effects of mutation rate in each replicating strategy is first illustrated in Figure 2. We show the time evolution of all the viral strands for each replication strategy using three different mutation rates. The genomic strands (solid line) achieve higher equilibrium concentrations than the antigenomic ones (dashed line) for the stamping machine kinetics. For geometric replication, however, the genomic and antigenomic strands asymptotically achieve identical equilibria. With $\mu = 0.1$ (Figure 2a) the master strands (black trajectories) achieve population equilibria higher than the mutant strands. If mutation is increased ($\mu = 0.3$; Figure 2b), the concentration of the mutant strands grows and master strands concentration decreases. For linear replication, the concentration of mutant genomic strands achieves a higher value than the antigenomic master strands.

For geometric replication, both master strands achieve higher populations than the mutant strands. If mutation rate is increased ($\mu = 0.75$) mutant strands dominate the population and the master ones have low population values (Figure 2c). We also computed the time evolution of the

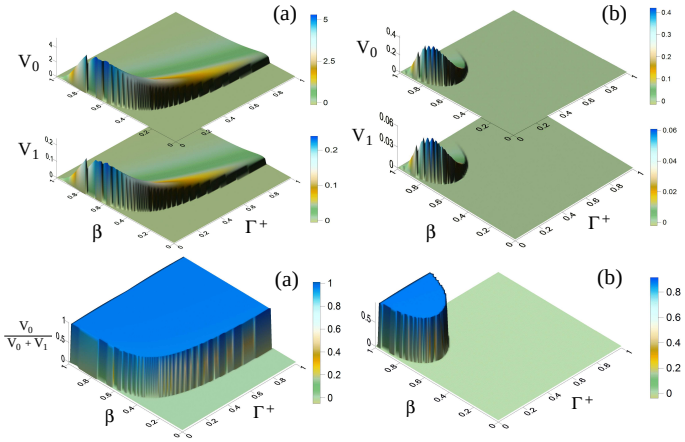

FIG. 5: Two different phases are present for the model, here defined on the (Γ^+, β) parameter space. The upper row shows the equilibrium of master and mutant virions, V_i. The lower row shows the fraction of virions containing non-mutated genomes. Parameters were set to $k_{20} = 0.75$, $k_{21} = 0.1$, $\varepsilon = 0.01$ and $\sigma = 10^{-4}$. Data are shown for values of mutation rate (a) $\mu = 0.2$ and (b) $\mu = 0.5$.

positive to negative strands ratio considering the master and the mutant strands of each polarity (see Figure 2d). For linear replication such a ratio is larger than one, indicating that there is much more production of positive-sense strands from the antigenomic templates. For geometric replication, this ratio evolves towards the unity value indicating that both positive and negative strands are synthesized at the same rates.

The stamping machine has a higher critical mutation rate. As expected, for linear replication the equilibrium concentration for both master genomic and antigenomic strands is asymmetric (Figure 3a and 3b). This actually means that we have a higher production of positive strands from the negative ones. On the contrary, the equilibrium concentrations for the master and the mutant strands are the

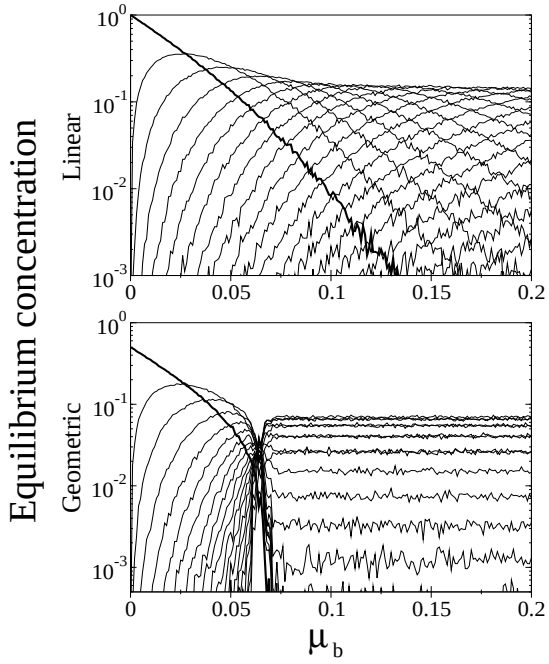

FIG. 6: Average equilibrium concentration of positive-sense strands in the bit string model. The per-bit mutation rate, μ_b, was used as tunable for linar (upper) and geometric (lower) modes with $\varepsilon = 0.01$ and $N(0) = 50$. In all the diagrams we show the normalized population numbers (averaging over 50 independent replicas when $\tau = 5000$) for genomic master strands (thick line) and their mutant spectrum (thin lines) containing the strands differing in one to twenty mutations from the master one.

same for both genomic and antigenomic sets. The critical mutation rate involving the entry into error catastrophe and the extinction of the master sequences is shown to be higher for linear replication (Figure 3a). For geometric replication, however, such a critical value is lower indicating that the viral strands are more sensitive to mutation (Figure 3b). The inset in Figure 3b illustrates the initial growth kinetics for each replication mode for the positive-sense strands (in linear-log scale). For geometric replication the initial growth phase is exponential. For the stamping machine strategy we obtain a subexponential growth kinetics.

The stamping machine is more robust to the accumulation of slightly deleterious mutations. Next, we sought to explore the effect of the severity of mutational effects on the accumulation of master and mutant strands of both polarities. The severity of mutations was computed as the ratio between the average replication rates of mutant strands Λ^+ and of the master strand Γ^+. This ratio will be one for neutral mutations ($\Lambda^+ = \Gamma^+$), and zero for lethal ones. Figure 4 shows the equilibrium population densities for each genomic class and their dependence on mutational severity. At relatively low mutation rates ($\mu = 0.15$) the positive master sequence remains dominant regardless the replication mode. As expected, strong effect mutations accumulate less than mild effect mutations irrespective of the mode of replication. However, geometric replication is more sensitive to the accumulation of mild mutations than stamping machine replication (Figure 4a), as indicated by the steeper slope for the positive master strands. A similar situation occurs at intermediate mutation rates ($\mu = 0.25$; Figure 4b): both replication modes accumulate more mild than strong effect mutations, with the geometric accumulating more mild mutations. At higher mutation rates ($\mu = 0.35$; Figure 4c) results remain similar for the stamping machine replication, that is, positive master genomes are still numerically dominant for all the range of mutation severities; however, geometric replication collapses at intermediate severities ($\Lambda^+ = 0.5$) and all genotypes get extinguished due to the excessive accumulation of small effect mutations.

Another difference between linear and geometric growth is that the second-most abundant genotype for lineal replication is the negative-sense master strand at low mutation rates irrespective of the severity of mutational effects, whereas negative-sense mutants are the second most abundant class for the geometric growth. At intermediate mutation rates, the positive-sense mutants become the second most abundant class when replication occurs via a stamping machine, and their frequency raises up as mutation rate increases. These results are in agreement to those presented in the previous section and support the notion that a stamping machine model of virus replication is not only compatible with higher mutation rates but also it is more robust to the severity of mutations.

Mature virion production. Our model also allows exploring other important features. For instance, we can analyze the production of viral particles using Γ^+ as control parameter thus analyzing different degrees of linear replication in mature virions production. We represent the mature viral particles, V, in the parameter space (β, Γ^+) for several mutation rates (Figure 5). We specifically differentiate between master, V_0, and mutant, V_1, virions, separating equation (7) in two new equations that account, respectively, for the formation of virions encapsidating either master or mutant genomic strands:

$$\frac{dV_i}{dt} = \varphi(x_i^+) - \sigma V_i, \quad i = 0, 1,$$

where the term $\varphi(x_i^+) = k_{2i}[(1-\beta)p]^m x_i^+$, being k_{2i} the encapsidation rate for the virions containing master ($i = 0$) and mutant ($i = 1$) strands. This distinction allows us to consider that the encapsidation rate is affected by mutation, setting $k_{20} = 0.75 > k_{21} = 0.1$. For this case equations (2), (3) and (5) are also modified to distinguish whether master or mutant genomes encapsidate at different rates. We show that when mutation rate is not very high ($\mu = 0.2$; upper row of Figure 5a), the maximum production of virions is mainly found for low values of Γ^+ and then the stamping machine replication is better than the geometric replication. Nevertheless, geometric replication is also producing virions at values of $\beta \approx 0.3$. This is not the case if mutation rate is increased, where the equilibrium concentration of virions is drastically reduced and confined to low values of Γ^+ (linear replication) and high values of β (upper row in Figure 5b).

We notice that increases in mutation rate are associated to decreases in the stationary concentration of the mature viri-

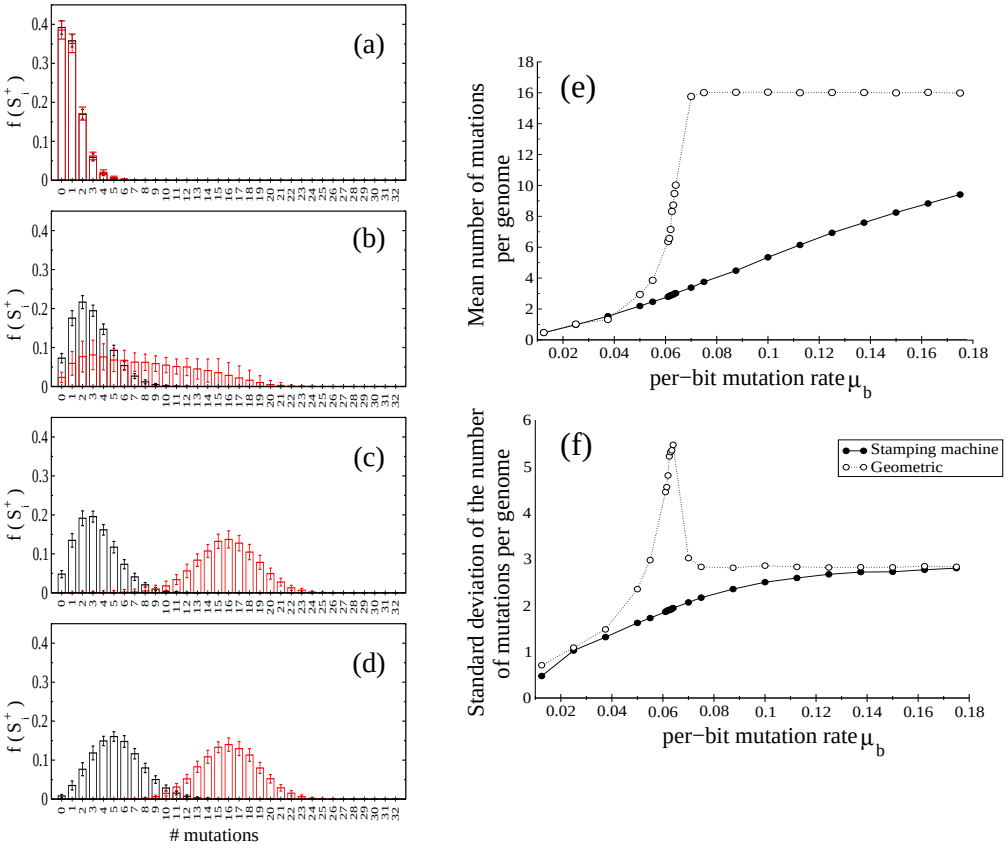

FIG. 7: (Left) Frequency distributions at equilibrium of the number of mutations per positive-sense strings, $f(S_i^+)$, and (right) statistical properties of the mutational load for several per-bit mutation rates. Four different frequency distributions are plotted as examples: (a) $\mu_b = 0.025$, (b) $\mu_b = 0.0625$, (c) $\mu_b = 0.07$ and (d) $\mu_b = 0.1$. In these histograms, both stamping machine and geometric replication strategies are represented in black and red, respectively. Each data point is the average ($\pm$ standard deviation) taken over 10^2 independent replicas. In (e) and (f) we show, respectively, the mean and the standard deviation of the number of mutations per genome obtained from the frequency distributions of mutant classes. In both plots linear and geometric replication modes are represented with black and open circles, respectively. Other relevant paramteres: $\varepsilon = 0.01$ and $N(0) = 50$.

ons. Moreover, the surface shown in the parameter space of Figure 5 considering V and thus same encapsidation rates for both master and mutant virions (i.e., without distinguishing between master and mutant virions and using equation (7)) has the same shape (results not shown). The lower row in Figure 5 shows the ratio of virions containing non mutated genomes, $V_0/(V_0 + V_1)$, also in the parameter space (β, Γ^+) for $\mu = 0.2$ and $\mu = 0.5$. It is shown that at increasing mutation rate this ratio decreases due to the higher production of mutant virions. Moreover, the region where no virions are produced is enlarged as mutation rate is increased and replication is closer to the geometric mode of replication.

Digital genomes

Geometric and linear replication show different transitions towards the error threshold. To analyze the effect of mutations in a Swetina-Schuster fitness landscape for both replication modes, we compute the equilibrium concentration for the master positive sequences and its mutant spectrum using the per-bit mutation probability, μ_b, with a degradation rate of $\varepsilon = 0.01$. The critical mutation probability, μ_b^c, is defined as the lowest mutation value involving the extinction of the master genomic strands, which is assumed to occur when $[S_i^+] < 10^{-4}$. We analyze two different initial conditions, a starting population with $N(0) = 50$ and $N(0) = 1$ positive-sense replicating master strands. The results are shown in Figure 6 for the analyses obtained using $N(0) = 50$. For both initial conditions linear replication displays a higher critical mutation, given by $\mu_b^c \approx 0.157$ and $\mu_b^c \approx 0.136$ for $N(0) = 50$ and $N(0) = 1$, respectively. For geometric replication this critical values are $\mu_b^c \approx 0.071$ (for an initial population of $N(0) = 50$) and $\mu_b^c \approx 0.069$ ($N(0) = 1$). We note that the diagram for geometric replication using a single strand as initial condition did not differ from the one obtained with $N(0) = 50$ (results not shown), and the critical mutation rate was almost the same. Indeed, even using a single initial genomic strand as a starting population, linear replication is more robust to mutation as compared with the geometric mode.

These results confirm that Luria's stamping machine is less sensitive to mutations. Moreover, the composition of the mutant spectrum is shown to be different according to the repli-

	Linear			Geometric						
μ_b	Mean	Median	SD	Mean	Median	SD	M-W	P	K-S	P
0.0125	0.462	0	0.47	0.473	0	0.71	-0.14	0.886	0.11	1
0.0250	0.975	1	1.02	1.020	1	1.09	-0.57	0.567	0.3	1
0.0375	1.532	1	1.31	1.321	1	1.48	-5.77	7.8×10^{-9}	3.16	0
0.0500	2.193	2	1.62	2.941	2	2.35	-6.31	2.7×10^{-10}	2.93	0
0.0550	2.465	2	1.72	3.855	3	2.97	-32.57	0	14.84	0
0.0610	2.789	3	1.86	6.368	5	4.45	-62.49	0	29.19	0
0.0615	2.846	3	1.88	6.571	6	4.55	-63.16	0	29.83	0
0.0620	2.869	3	1.89	7.147	6	4.80	-68.42	0	32.87	0
0.0625	2.907	3	1.90	8.315	8	5.22	-24.74	0	12.09	7.3×10^{-8}
0.0630	2.932	3	1.91	8.724	8	5.31	-80.81	0	39.86	0
0.0635	2.992	3	1.93	9.472	9	5.34	-87.09	0	43.18	0
0.0640	3.022	3	1.94	10.02	10	5.46	-90.18	0	43.18	0
0.0700	3.384	3	2.06	15.76	16	3.02	-122.1	0	45.26	0
0.0750	3.755	4	2.17	16.01	16	2.83	-38.74	0	21.86	0
0.0875	4.482	4	2.35	16.03	16	2.81	-38.67	0	21.57	0
0.1000	5.345	5	2.50	16.04	16	2.86	-38.48	0	21.14	0
0.1125	6.147	6	2.59	16.00	16	2.83	-38.24	0	20.6	0
0.1250	6.931	7	2.67	16.02	16	2.82	-37.82	0	20.07	0
0.1375	7.589	7	2.72	16.02	16	2.82	-37.35	0	19.41	0
0.1500	8.243	8	2.72	15.99	16	2.82	-36.71	0	18.54	0
0.1625	8.829	9	2.77	16.03	16	2.84	-35.84	0	17.86	0
0.1750	9.412	9	2.80	15.98	16	2.83	-34.70	0	16.94	0

TABLE II: Statistics describing the mutational load of viral quasispecies generated by linear and geometric modes of replication for increasing values of μ_b. SD: Standard deviation; M-W: Mann-Whitney statistic; K-S: Kolmogorov-Smirnov statistic.

cation strategy. It is well known that for geometric growth the mutant spectrum suffers a sharp phase transition at the error threshold, and each mutant genome reaches a steady-state concentration that only depends on its mutational coupling (9). However, we show that this is not the case for the stamping machine replication, since a sharp phase transition is never observed and different genomes rise and decrease in frequency depending on mutation rate (Figure 6, upper).

Statistical analysis of the distribution of the number of mutations per genome. Next we sought to explore the effect of the two extreme models of RNA virus replication on the mutational load of newly generated viral populations. Figure 7 shows the distribution of mutations accumulated in genomic strands for a set of representative μ_b values as a function of the mode of replication. Table II shows the detailed statistical analyses for μ_b varying from 0.0125 to 0.175. At very low mutation rates ($\mu_b = 0.025$) both replication mechanisms produced distributions of mutants that were undistinguishable (Figure 7a) both in the average number of mutations and in shape (Table II). However, for $\mu_b > 0.025$ the mutant distributions generated quickly diverged both in their average values and shapes (Table II), with the geometric replication generating a much larger mutational load, with distributions centered on higher values (Table II). As illustrated in Figure 7e, the average number of mutations per genome accumulated under the stamping machine mechanisms steadily increased until reaching a maximum value of 9.412 ± 2.803.

Similarly, the standard deviation of the number of mutations per genome also increased in a similar way (Figure 7f). By contrast, the average number of mutations per genome produced by the geometric replication increased much faster and reached a plateau of 16 mutations per genome for $\mu_b \geq 0.075$ (Table II and Figure 7e). We also computed the maximum number of mutations per genome at equilibrium from 50 independent replicas at increasing mutation rates (results not shown). For low values of mutation rate ($0 \leq \mu_b \leq 0.028$) both replication modes showed a similar low maximum number of mutations. For higher mutation rates, the geometric model rapidly increased in the maximum number of mutations, with some strands carrying up to 23 mutations for $\mu_b = 0.056$. Linear replication generated, for the same mutation rate, a maximum load of 13 mutations per genome. Actually, in the range $0.068 \leq \mu_b \leq 0.18$, the maximum number of mutations for geometric replication was between 27 and 29, while for linear replication such a number fluctuated between 15 and 24 mutations. The variance in mutational load for geometric replication also increased faster than in the case of linear replication mechanism. However, this fast increase was only transient and until the point in which the average mutational load reached its maximum value. Afterwards, the variance in the number of mutations sharply decreased and asymptotically approached the variance value observed for the stamping machine model (see Figure 7f).

As described in the Introduction, under a purely stamping

machine mechanism, the number of mutations per genome should conform to a Poisson distribution, whereas for a geometric mechanism the distribution departs from the Poisson model and fits the more complex Luria-Delbrück distribution. To confirm this expectation, we run Kolmogorov-Smirnov tests for the null hypothesis of the Poisson distribution (data shown in Table III). As expected, under the stamping machine model, the distributions of mutations per genome were Poisson for all values of μ_b whereas they departed from this null model for values of $\mu_b \geq 0.0375$.

	Linear		Geometric	
μ_b	K-S	P	K-S	P
0.0125	0.09	1	0.20	1
0.0250	0.37	0.999	0.75	0.625
0.0375	0.58	0.895	3.54	0
0.0500	0.89	0.404	3.15	0
0.0550	0.93	0.352	4.35	0
0.0610	1.07	0.206	6.31	0
0.0615	1.08	0.190	6.39	0
0.0620	1.19	0.115	6.45	0
0.0625	1.15	0.140	6.69	0
0.0630	1.11	0.170	6.66	0
0.0635	1.08	0.195	6.15	0
0.0640	1.18	0.123	6.09	0
0.0700	1.12	0.165	2.52	0
0.0750	1.06	0.210	2.72	7.4×10^{-7}
0.0875	1.08	0.197	2.74	5.87×10^{-7}
0.1000	0.75	0.632	2.67	1.26×10^{-6}
0.1125	0.44	0.990	2.72	7.12×10^{-7}
0.1250	0.23	1	2.81	2.65×10^{-7}
0.1375	0.36	1	2.78	3.89×10^{-7}
0.1500	0.63	0.826	2.72	7.5×10^{-7}
0.1625	0.77	0.588	2.68	1.16×10^{-6}
0.1750	0.90	0.389	2.75	5.15×10^{-7}

TABLE III: Fit of the average number of mutations accumulated by viral populations replicating linearly or geometrically, at increasing μ_b, to the null hypothesis of a Poisson distribution. K-S: Kolmogorov-Smirnov statistic.

DISCUSSION

It is known that the mode of virus replication can change the rates at which deleterious mutations accumulate. Depending on whether genomes replicate linearly or geometrically one may observe different fractions of mutation-free genomes. Linear replication, also known as Luria's stamping machine (3), implies that the copies produced during the first round of replication will be the only templates for the generation of the entire quasispecies. Experimental data suggest that $\phi X174$ replicates linearly (6). However, if replication is geometric, as experimentally found for the phage $T2$ (3), all the synthesized copies during infection will serve as templates in the following generations. Intermediate situations have also been described for other viruses (1). As far as we know, previous attempts to model viral replication have only investigated the geometric case. Moreover, the majority of theoretical work on quasispecies did not consider the genomic-antigenomic duality of the sequences.

In this work we analyze a structured model describing the single-cell reproductive cycle of positive-sense RNA viruses that make no subgenomic mRNAs and encode a single polyprotein that is selfprocessed into structural and nonstructural components. We develop a mathematical model using as key variables the genomic and antigenomic RNA strands, the viral polyprotein precursor, the translational complexes formed by viral RNA and cellular ribosomes, and the mature virions. Genetic heterogeneity is introduced with a simplified quasispecies structure of the strands considering master sequences (which have the higher fitness) and the pool of deleterious mutants for each strands polarity, which are grouped into a single variable denoting an average mutant sequence different from the master one. We analyze a single-peak fitness landscape (21) which assumes that mutations have a large deleterious effect. We explore the error threshold and the sensitivity to mutations for a viral populations replicating linearly or geometrically.

We have shown that the error catastrophe takes place at a higher mutation rate for the stamping machine mechanism, indicating that this strategy is less sensitive to the effect of deleterious mutations. On the contrary, geometric replication displays a lower critical mutation rate, being more sensitive to mutation. Consistently, we have also shown that mild mutational effects tend to accumulate more in the geometric case, and that under such a growth kinetics the population collapses at intermediate mutation rates. However, the stamping machine strategy is less sensitive to the accumulation of mild mutations and viral strands continue existing for mutation rates that produce a collapse of viral populations replicating geometrically. Additionally, the production of mature virions also has a strong dependence on the mode of replication. For low mutation rates, the maximum amount of virions is produced with linear replication, although for certain values of the fraction of replicase produced ($\beta \approx 0.3$) geometric replication also induces the production of virions at low mutation rates. Nevertheless, if mutation rate is increased, a combination of linear replication and high amount of replicase ensures the (lower) production of virions. This is not the case for geometric replication, where no mature virions are produced at all.

To complement the analysis of the mathematical model we also used a model of digital genomes which considers the intrinsic noise due to small population sizes, also explicitly considering the heterogeneous structure of the quasispecies and the duality of the strands. This model consistently shows that the critical per-bit mutation rate is higher for the linear case and the mutational load lower.

Whether RNA viruses may have evolved some mechanisms to buffer the deleterious effects of mutations has attracted the attention of researchers (27). Robustness is defined as a reduced sensitivity to perturbations affecting phenotypic ex-

pression. RNA virus populations, may owe their robustness to several of the following mechanisms ((27) and references therein). First, individual hypersensitivity to mutational effects translates into robustness at the population level as a consequence of a more efficient purifying selection that maintains average fitness high. Second, high mutation rates characteristic of RNA viruses may impose a strong selective pressure that pushes virus populations towards regions of the sequence space where the density of neutral mutations is higher. Third, the variable and random ploidy of viruses and the frequent coinfection events enhance the possibility of genetic complementation. Fourth, segregation of segments during mixed infections and homologous recombination are forms of sex that may recreate mutation-free genomes. Fifth, cellular buffering mechanisms (e.g., heat-shock proteins) can be utilized by the viruses in their own benefit as an extrinsic source of robustness. The results reported in this study suggest that, in addition to these five potential mechanisms, by choosing a stamping machine mode of replication, RNA viruses will also accumulate less deleterious mutations, will have a higher critical mutation rate and will suffer in a lesser extent from the effect of deleterious mutations, that is, increase their robustness.

Acknowledgments

This work has been supported by the Human Frontier Science Program Organization grant RGP12/2008. Work in València was also funded by the Spanish Ministerio de Ciencia e Innovación grant BFU2006-14819-CO2-01/BMC. We also acknowledge support from The Santa Fe Institute.

[1] L. Chao, C. U. Rang, and L. E. Wong. Distribution of Spontaneous Mutants and Inferences about the Replication Mode of the RNA Bacteriophage $\phi 6$. *J. Virol.*, 76(7):3276–81, 2002.

[2] R. French and D. C. Stenger. Evolution of Wheat Streak Mosaic Virus: Dynamics of Population Growth Within Plants May Explian Limited Variation. *Annu. Rev. Phytopathol.*, 41:199–214, 2003.

[3] S. E. Luria. The frequency distribution of spontaneous bacteriophage mutants as evidence for the exponential rate of phage production. *Cold Spring Harbor Symp Quant Biol*, 16:463–470, 1951.

[4] A. Dewanji, E. G. Luebeck, and S. H. Moolgavkar. A generalized Luria-Delbruck model. *Math Biosci*, 197:140–152, 2005.

[5] J. M. Malpica, A. Fraile, I. Moreno, C. I. Obies, J. W. Drake, and F. García-Arenal. The rate and character of spontaneous mutation in an RNA virus. *Genetics*, 162:1505–11, 2002.

[6] D. Denhart and R. B. Silver. An analysis of the clone size distribution of $\phi X174$ mutants and recombinants. *Virology*, 30:10–19, 1966.

[7] S. F. Elena, P. Agudelo-Romero, P. Carrasco, S. Codonẽr, F. M. Martín, C. Torres-Barceló, and R. Sanjuán. Experimental evolution of plant RNA viruses. *Heredity*, 100:478–483, 2008.

[8] E. Domingo, E. Baranowski, C. M. Ruiz-Jarabo, A. M. Martín-Hernández, J. C. Sáiz, and C. Escarmís. Quasispecies structure and persistence of RNA viruses. *Emerging Infect. Dis.*, 4(4):521–527, 1998.

[9] M. Eigen, J. McCaskill, and P. Schuster. The molecular quasispecies. *Adv Chem Phys*, 75:149–263, 1989.

[10] Y. Sidorenko and U. Reichl. Structured model of Influenza Virus Replication in MDCK Cells. *Biotech. and Bioeng.*, 88(1):1–14, 2004.

[11] M. Eigen, C. K. Biebricher, M. Gebinoga, and W. C. Gardiner. The hypercycle. Coupling of RNA and protein synthesis in the infection cycle of an RNA bacteriophage. *Biochemistry*, 30(46):11005–11018, 1991.

[12] D. C. Krakauer and N. L. Komarova. Levels of selection in positive-strand virus dynamics. *J. Evol. Biol.*, 16:64–73, 2003.

[13] R. Srivastava, L. You, J. Summers, and J. Yin. Stochastic vs. Deterministic Modeling of Intracellular Viral Kinetics. *J. theor. Biol.*, 218:309–21, 2002.

[14] V. P. Zhdanov. Bifurcation in a generic model of intracellular viral kinetics. *J. Phys. A: Math. Gen.*, 37:L63–L66, 2004.

[15] D. Endy, D. Kong, and J. Yin. Intracellular kinetics of a growing virus: A genetically structured simulation for the bacteriophage T7. *Biotechnol Bioeng*, 55:375–89, 1997.

[16] L. You, P. F. Suthers, and J. Yin. Effects of *Escherichia coli* physiology on growth of phage T7 in vivo and in silico. *J Bacteriol*, 184:1888–94, 2002.

[17] B. Reddy and J. Yin. Quantitative intracellular kinetics of HIV type 1. *AIDS Res Hum Retroviruses*, 15:273–83, 1999.

[18] H. Dahari, R. M. Ribeiro, C. M. Rice, and A. S. Perelson. Mathematical Modeling of Subgenomic Hepatitis C Virus Replication in Huh-7 Cells. *J. Virol.*, 81(2):750–760, 2007.

[19] K. Lim, V. Lang, T. Lam, and J. Yin. Model-Based Design of Growth-Attenuated Viruses. *PLoS Computational Biology*, 2(9), 2006. e116. DOI: 10.137/journal.pcbi/0020116.

[20] L. A. Ball. *Fields Virology*, chapter 5. Replication Strategies of RNA Viruses. Lippincott Williams & Wilkins, 1995. Fourth Edition.

[21] J. Swetina and P. Schuster. Self-replication with errors. A model for polynucleotide replication. *Biophys. Chem.*, 16:329, 1982.

[22] J. Sardanyés, S. F. Elena, and R. V. Solé. Simple quasispecies models for the survival-of-the-flattest effect: the role of space. *J. theor. Biol.*, 250(3):560–568, 2008.

[23] R. V. Solé, J. Sardanyés, J. Díez, and A. Mas. Information catastrophe in RNA viruses through replication thresholds. *J. theor. Biol.*, 240(3):353–359, 2006.

[24] I. Leuthäusser. An exact correspondence between Eigen's evolution model and a two-dimensional Ising system. *J Chem Phys*, 84(3):1884–5, 1986.

[25] I. Leuthäusser. Statistical mechanics of Eigen's evolution model. *J Stat Phys*, 48:343–360, 1987.

[26] S. H. Strogatz. "Nonlinear Dynamics and Chaos with applications to Physics, Biology, Chemistry, and Engineering". Westview Press, 2000.

[27] S. F. Elena, P. Carrasco, J. A. Daròs, and R. Sanjuán. Mechanisms of genetic robustness in RNA viruses. *EMBO Rep*, 7:168–173, 2006.